Carbon steel corrosion inhibition in H2SO4 0.5 M medium by thiazole-based molecules: Weight loss, electrochemical, XPS and molecular modeling approaches

O. Benali, M. Zebida, F. Benhiba, A. Zarrouk, Ulrich Maschke

Carbon steel corrosion inhibition in H_2SO_4 0.5 M medium by thiazole-based molecules: Weight loss, electrochemical, XPS and molecular modelling approaches

O. Benali[1]*, M. Zebida[1], F. Benhiba[2,3], A. Zarrouk[3], U. Maschke[4]

[1]*Laboratory of Chemistry: Synthesis, Properties and Applications, University of Saida –Dr. Moulay Tahar, Algeria.*

[2]*Laboratory of Advanced Materials and Process Engineering, Faculty of Sciences, Ibn Tofail University, BP 242, 14000, Kenitra, Morocco.*

[3]*Laboratory of Materials, Nanotechnology and Environment, Faculty of Sciences, Mohammed V University in Rabat, P.O. Box 1014 Agdal-Rabat, Morocco.*

[4]*Unité Matériaux et Transformations: Ingénierie des systèmes polymères (UMET :ISP), Université Lille1, France.*

Corresponding author: benaliomar@hotmail.com

Abstract

Carbon steel (CS) corrosion prevention is a significant problem in the industry. The development of an effective protection strategy is a popular research area. In this work, three thiazole derivatives (3-(2-methoxyphenyl)-4- methylthiazol-2(3H)-thione (P1), 3-phenyl-4-methylthiazol-2(3H)-thione (P2) and 3-(2-methyl-phenyl)-4-methylthiazol-2(3H)-thione (P3)) were used in 0.5 M H_2SO_4 solution for CS corrosion mitigation. Weigh loss and electrochemical tests were used to assess their corrosion prevention effectiveness, while X-ray photoelectron spectroscopy was used to examine the steel surface (XPS). Electrochemical

tests showed an inhibition efficiency between 90.1% and 98.4% for CS exposed to acidic solution containing 2×10^{-4} M of the three thiazole derivatives. The three inhibitors were categorized as mixed type inhibitors since they inhibited both cathodic and anodic corrosion and they follow the Langmuir isotherm. XPS showed that inhibitor molecules formed a stable layer on steel surface through chemical and physical interactions. Furthermore, these experimental outcomes are well complemented from results analysed by quantum chemistry calculations. Additionally, MD simulation outcomes helped in visualization of the adsorbed configuration of these compounds on the metal surface.

Keywords: Thiazole derivatives; Carbon steel corrosion; Adsorption; XPS; Theoretical approach.

1. Introduction

Metal corrosion has been seen as a major problem in many industries. During the corrosion awareness day, it was pointed out that the annual cost of corrosion amounted to US $ 2,500 billion [1] making the protection of assets against corrosion is essential. However, this cost can be reduced if the use of highly efficient corrosion reduction technologies is made. One such method to control metallic corrosion is the use of inhibitors [2-12] in acidic medium. The literature reveals that the presence of hetero-atoms, non-bonding electrons and π-electrons make the organic compound an efficient corrosion inhibitor [13-16]. Thiazolic and their derivatives have been shown to be good inhibitors. This is due to their polar groups and potential for complexation with the metal surface. In addition, they exhibit different pharmacobiological properties [17-20]. The objective of this study is to evaluate the anticorrosion performance of three synthesized thiazolic compounds, namely 3-(2-methoxyphenyl)-4- methylthiazol-2(3H)-thione (P1), 3-phenyl-4-methylthiazol-2(3H)-thione (P2) and 3-(2-methyl-phenyl)-4-methylthiazol-2(3H)-thione (P3) using weight loss measurement and electrochemical techniques (polarization curves and impedance

2

spectroscopy). The carbon steel surface was also examined by X-ray photoelectron spectroscopy (XPS). Quantum chemistry calculations and molecular dynamic simulation (MD) have been established.
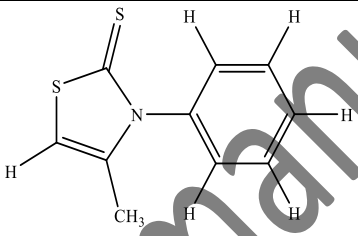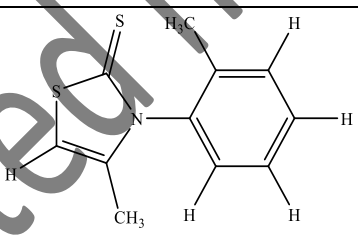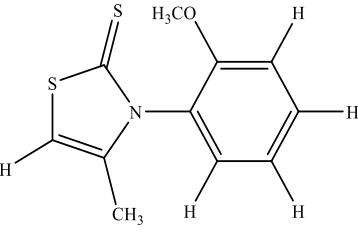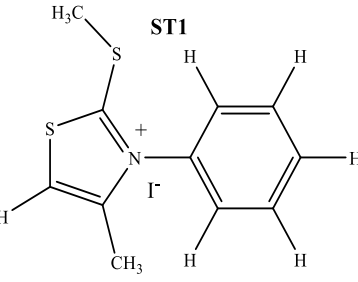
2. Materials and Methods

2.1 Inhibitors

See Table 1.

Table 1

Nomenclature of molecules, their structures and abbreviated names.

Nomenclature	Molecular structure	abbreviation
3-phenyl-4-methylthiazol-2(3H)-thione		**P1**
3-(2-methyl-phenyl)-4-methylthiazol-2(3H)-thione		**P2**
3-(2-methoxyphenyl)-4-methylthiazol-2(3H)-thione		**P3**
4-methyl-2-(methylthio)-3-phenylthiazol-3-ium iodide		IE= 95.25% to 10^{-3} M in 0.5 M H_2SO_4 (T = 303 K and 1 h of immersion) for comparison by DFT and Molecular simulation [13]

3

2.2 Material and solution

The detailed description of the nature of the steel, its preparation as well as the acid solution used during this study was given in one of our works published previously [13].

2.4 Weight Loss tests

Weight loss measurement was used to evaluate the inhibition action of the three inhibitors. The corrosion rate (*C.R.*) and inhibition efficiency (*EI$_{CR}$%*) were calculated from Eqs. (1) and (2) :

$$C.R. = \frac{m_0 - m_i}{S \times t} \tag{1}$$

where m$_0$ and m$_i$ are the mass of carbon steel before and after immersion, *S* its and *t* is the time of immersion (1 h).

$$EI_{CR}\left(\%\right) = 1 - \frac{CR_i}{CR_0} \tag{2}$$

where *C.R$_i$* and *C.R$_0$* are corrosion rate of the carbon steel with and without inhibitors, respectively.

2.5 Electrochemical Studies

The performance of **P1**, **P2** and **P3** on carbon steel in 0.5 M H$_2$SO$_4$ was performed by electrochemical methods. A standard three-electrode cell (carbon steel as working electrode, saturated calomel electrode as reference electrode and platinum as counter electrode) was used. The electrochemical system is composed of an electrochemical cell connected to a potentiostat (Versastat) controlled by Volta master 4 software. The immersion time of the electrochemical tests was 1h (to reach the equilibrium state). The polarization curves were produced by applying a potential range going from -700 to -300 mV with a scan rate equal of 0.5 mV/s. The potentiodynamic polarization parameters were determined by extrapolation from the cathodic part to the corrosion potential. Electrochemical impedance spectra (EIS)

4

were obtained by scanning frequency from 10^5 Hz to 0.1 Hz at corrosion potential with an alternating current of $\pm$ 10 mV of amplitude.

IE of potentiodynamic polarization measurement was defined as:

$$EI_{i_{corr}} \left(\% \right) = \frac{i_{corr} - i_{corr(inh)}}{i_{corr}} \times 100 \tag{3}$$

where i_{corr} and $i_{corr(inh)}$ are the current density values in absence and in presence of the inhibitors, respectively.

EI of EIS measurements was defined as:

$$EI_{R_p} \left(\% \right) = \frac{R_{p(inh)} - R_p}{R_{p(inh)}} \times 100 \tag{4}$$

where $R_{p(inh)}$ and R_p are the charge transfer resistance of inhibited and uninhibited solutions.

2.6. X-ray photoelectron spectroscopy (XPS) analysis

The detailed study of the XPS part was done according to the protocol mentioned in one of our previous article [16]. In this present work it has been presented that the results of the best inhibitor P1 ($2x10^{-4}$M).

2.7 DFT and Molecular simulation details

DFT method has been carried for **P1**, **P2, P3** and **ST1** in order to provide more details on the electronic behaviour at the molecular structure level of these compounds [21]. This method was performed in order to correlate the inhibitory efficiency obtained experimentally with the quantum descriptors found theoretically [22]. The lowest energy inhibitor shapes were tested in the DFT calculations conducted under pressure and in the aqueous phase. Additionally, the molecular structures of the compounds studied have been optimized to the final geometry by means of the Gaussian 09 software suite at the DFT level in a functional B3LYP implementing a 6-31G (d, p) basis set [23].

5

The quantum descriptors like energy frontier molecular orbitals (E_{LUMO} and E_{HOMO}), gap energy (ΔE_{gap}), electronegativity "χ" , global hardness "η", fraction of electrons transferred from the inhibitor molecule to the metal surface "ΔN_{110}" calculated using the equations used in our previously published work [24].

The adsorption of the molecules onto the Fe (1 1 0) was established using the molecular dynamics simulation. This process was performed using the Forcite module which is integrated in the materials studio[2016] software [25-26]. The study of these interactions of the molecules with the Fe (1 1 0) surfaces was carried out from a simulation box (22.34 * 22.34 * 36.13 $\mathring{A}^3$) with periodic boundary conditions. The Fe (1 1 0) surface was presented with a 6-couche slab model in each layer representing a (9×9) unit cell. The constructed simulation box is emptied by 24.14 $\mathring{A}^3$. This vacuum is occupied by $500H_2O$, $10H_3O^+$, $5SO_4^{2-}$ and the inhibitory molecule. The temperature of the simulated system of 303 K was controlled by the Andersen thermostat, NVT ensemble, with a simulation time of 400 ps and a time step of 1.0 fs, all under the COMPASS force field [27].

3. Results and Discussion

3.1 Weight Loss Measurements

3.1.1. Effect of concentration

The variation of the weight loss (1 hour of immersion) at 303 K is displayed in Table 2.

Table 2

Effect of concentration of **P1**, **P2** and **P3** in 0.5 M H_2SO_4.

Inhibitors	*Conc.* *(M)*	*C.R.* *(mg cm^2 h^{-1})*	*IE$_{CR}$ (%)*
	Blank	6.65	----
	1×10^{-6}	5.34	19.7
	1×10^{-5}	3.19	52.0
P1	1×10^{-4}	1.25	81.1
	2×10^{-4}	0.33	95.0
	Blank	6.65	----

	5×10^{-6}	4.40	33.8
P2	1×10^{-5}	3.80	42.8
	1×10^{-4}	1.99	70.0
	2×10^{-4}	0.57	91.3
	Blank	6.65	----
	5×10^{-6}	4.07	38.6
P3	1×10^{-5}	2.69	59.4
	1×10^{-4}	1.96	70.5
	2×10^{-4}	1.11	83.2

Even though weight loss are primary results, they are of great interest and give basic insights about the performance of tested compounds. Based on this finding, we could obviously assume that tested thiazole derivatives act by adsorption on the steel surface, which can be favored by the presence of several nonbonding electrons on heteroatoms of functional groups ($-CH_3$, $-OCH_3$), and π-electrons of the aromatic rings. From Table 2, we can notice that the corrosion rates of carbon steel gradually decrease with the increase of the amount of inhibitors. This behavior is generally attributed to their adsorption on the active sites of the surface of carbon steel, which limits the dissolution of metal with a decrease in the corrosion rate. It should be noted that the inhibition rates of the three compounds follows the order **P1 > P2 > P3**. The presence of the two OMe and = S groups on the same side in the most stable conformation (in **P3**) leaves a steric gene between the non-binding oxygen electron and the non-binding sulfur electron, which influences the flatness of the molecule as well as its adsorption on the metal surface. All of this will appear clearly on the effectiveness of the **P3** molecule.

3.1.2 Effect of immersion time

To better visualize the effect of the aggressive solution on the corrosion rate of the carbon steel studied and its inhibition, we examined the evolution of the gravimetric parameters at different immersion times for the optimal concentration (2×10^{-4} M) of **P1**. The measurements

7

were taken for different immersion times ranging from t = 1 to 24 hours. The results obtained are presented in the Table 3.

Table 3

Corrosion rates and inhibitory efficiencies for different immersion times for **P1** at 2×10^{-4} M in 0.5 M H_2SO_4 for corrosion of carbon steel at 303 K.

Immersion times (h)	Conc. (M)	C. R. ($mg\ cm^2\ h^{-1}$)	IE_{CR} (%)
1	Blank	6.65	----
	2×10^{-4}	0.33	95.0
2	Blank	7.64	----
	2×10^{-4}	0.34	95.5
4	Blank	6.40	----
	2×10^{-4}	0.24	96.2
8	Blank	6.65	----
	2×10^{-4}	0.25	96.2
24	Blank	6.65	----
	2×10^{-4}	0.27	95.9

From the Table 3, it is mentioned that the corrosion rate of blank solution increases after an immersion of 2 hours. This value decreases again then it stabilizes towards a constant value (6.65 mg/cm^2). This decrease in corrosion rates without inhibitor is due to the adsorption of corrosion product to the steel surface. In the presence of **P1**, the corrosion rate remains almost constant at first immersion, and then it decreases slightly. Regarding the inhibition efficiency, we note that their values are greater than 95% for the all immersion time, which confirms the stability of the film formed by the inhibitor molecules and its adhesion [28].

3.1.3. Effect of temperature

The temperature effect is very important in the corrosion study, because an increase in temperature accelerate the dissolution of metals [29-30]. The gravimetric measurements in 0.5 M of the H_2SO_4 acid solution obtained at different amounts of **P1** are established (Table 4). It can be seen from this table that the corrosion rate in the presence of inhibitor

8

concentration is less than those obtained in the blank solution indicating the adsorption behavior of **P1** molecules [31]. Also, it shows a significantly decreases in the inhibition efficiency with the rise of temperature from 303 K to 318 K, indicating the inhibitor is prone to desorb from the surface at higher temperature [32].

Table 4

Corrosion rates and inhibitory efficiencies of **P1** at different temperatures

| Temperature (K)	Conc. (M)	C.R. ($mg\ cm^2\ h^{-1}$)	IE_{CR} (%)
	Blank	6.65	----
	1×10^{-6}	5.34	19.7
303	1×10^{-5}	3.19	52.0
	1×10^{-4}	1.25	81.1
	2×10^{-4}	0.33	95.0
	Blank	9.58	----
	1×10^{-6}	7.78	18.8
308	1×10^{-5}	6.57	30.4
	1×10^{-4}	4.15	56.6
	2×10^{-4}	1.40	85.4
	Blank	12.62	----
	1×10^{-6}	10.41	17.5
313	1×10^{-5}	8.87	29.7
	1×10^{-4}	7.56	50.2
	2×10^{-4}	3.60	71.5
	Blank	17.93	----
	1×10^{-6}	14.78	17.1
318	1×10^{-5}	11.64	25.1
	1×10^{-4}	9.37	47.7
	2×10^{-4}	6.00	66.5

3.1.4. Activation parameters

The values of activation energy (E_a) of carbon steel in aggressive solution calculated through Arrhenius equations [33].

$$C.R. = A \times e^{\frac{-E_a}{R \times T}} \tag{5}$$

where R = 8.314 J/mol.K, A is pre-exponential factor and *T* is the temperature (K).

9

The logarithmic transformation of the equation 5 for all concentration is given in Figure 1 and the obtained results are presented in Table 5.
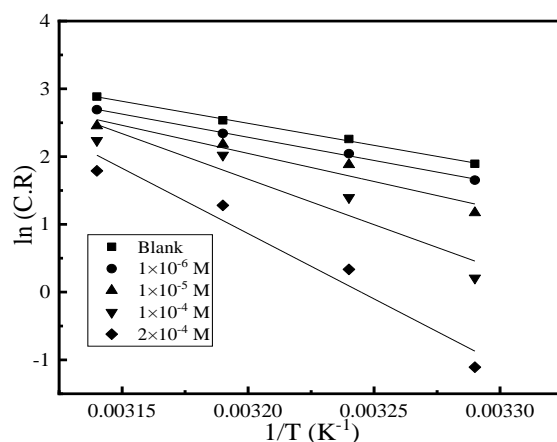
Fig. 1. Arrhenius plots of carbon steel in absence and in presence of **P1**.

The comparison of the activation parameters acquired without (E_a) and with **P1** (E_a^{inh}) predicts the dependence of the protective power of the inhibitor on the temperature and the classifier according to the classification proposed by Radovici [34-35]:

- Inhibitors for which $E_a^{inh} > E_a$ adsorbs to the substrate through weak bonds of an electrostatic nature. This type of bond is temperature sensitive and does not effectively fight against corrosion when the temperature rises.

- Inhibitors for which $E_a^{inh} < E_a$ present their protective power increase with temperature. These inhibitors are the most effective since they adsorb to the metal surface by chemical adsorption.

- Inhibitors for which $E_a^{inh} \sim E_a$, Very few compounds belong to this category which does not show changes in inhibitory power with temperature.

Table 5

Values of E_a of carbon steel in the absence and presence of **P1**.

Conc. (M)	E_a (kJ/mol)
Blank	54.07
1×10^{-6}	56.90
1×10^{-5}	68.94
1×10^{-4}	111.59
2×10^{-4}	160.26

In addition, the activation energies obtained with **P1** are higher than those obtained in the case of aggressive solution alone. The increase in energy activation in the presence of our compound is attributed to this the physisorption on the metal surface [36-37]. This result clearly indicates that the addition of **P1** to the corrosive medium implies a higher energy for overcome the energy barrier of the dissolution reaction of steel due to the formation of a protective film, which hinders the access of corrosive ions to the surface and therefore decreases the rate of corrosion of the metal. Other researchers have reported similar results as part of their studies on the corrosion inhibition of steel in sulfuric acid by thiazole derivatives [38-39].

Table 6

Comparative values of activation energy reported in the case of carbon steel in 0.5 M H_2SO_4.

| E_a (kJ/mol)	Reference	E_a (kJ/mol)	Reference
160.26 (2×10^{-4} M)	This work	105.0 (100 ppm)	[33]
131.0 (100 ppm)	[33]	119.88 (10^{-3} M)	[40]
151.2 (100 ppm)	[33]	78.98 (10^{-3} M)	[40]
122.4 (100 ppm)	[33]	76.95 (10^{-3} M)	[41]

3.2 Potentiodynamic polarization

The monitoring of the progression and mechanism of electrochemical reactions (the anodic and cathodic) as well as the identification of the effect of the concentration of the inhibitor on the latter is generally done by the method of potentiodynamic polarization. Tafel curves for

11
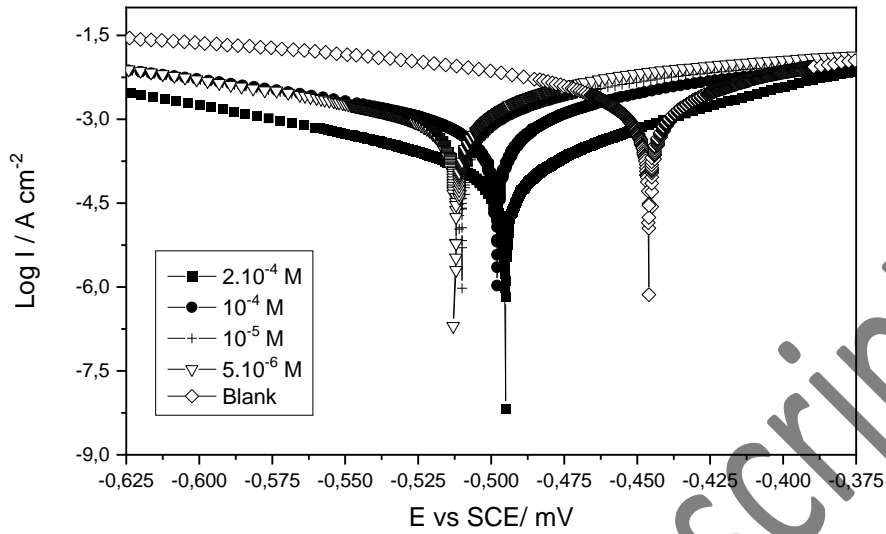
carbon steel in 0.5 M H₂SO₄ in the presence of **P1, P2** and **P3** are presented in Figures 2a, 2b and 2c, respectively.
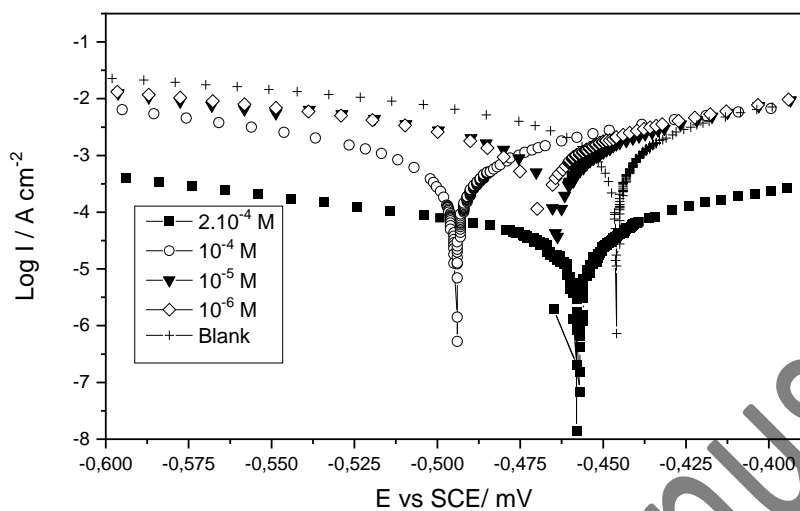
Fig. 2a. Polarization curves of carbon steel / **P1**/ 0.5 M H₂SO₄ system at 303 K.
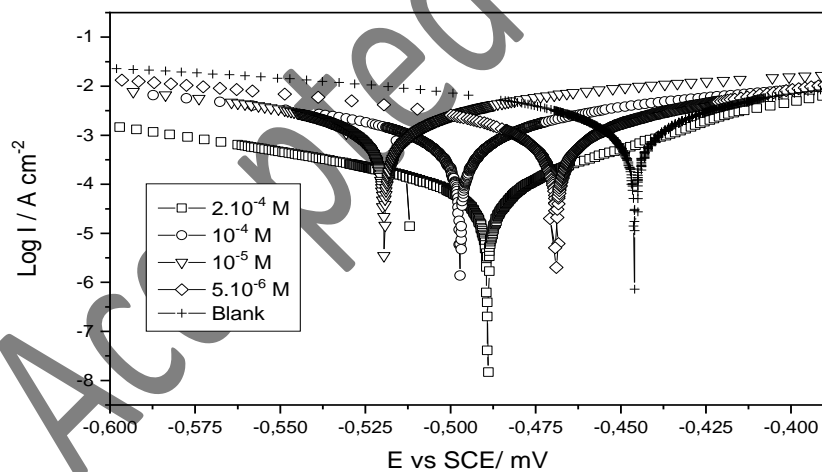
Fig. 2b. Polarization curves of carbon steel / **P2**/ 0.5 M H₂SO₄ system at 303 K.

Fig. 2c. Polarization curves of carbon steel / **P3**/ 0.5 M H₂SO₄ system at 303 K.

The Electrochemical including corrosion potential (E_{corr}), current density (i_{corr}), Tafel slopes (b_c and b_a), inhibition efficiency (IE_{icorr}) and corrosion rate (C_R) are displayed in Table 7.

The corrosion rate could be estimated using corrosion current density as:

$$CR = 3.27\ i_{corr}\ (Eq.w/\ d) \tag{6}$$

where, i_{corr} denotes the value of corrosion current density in mA.cm^{-2}, Eq. Wt. while d represents the equivalent weight and density of mild steel respectively.

In this work we have also correlated polarization resistance using the Stern–Geary equation (7):

$$R_p = \frac{b_c b_a}{2.303.i_{corr}\ (b_a + b_a)} \tag{7}$$

where ba and bc are the anodic and cathodic Tafel slopes and i_{corr} the corrosion current density in mA.cm^{-2}.

The values of Rp are also given in table 7.

13

Table 7. Electrochemical parameters for carbon steel /0.5 M H_2SO_4 with **P1**, **P2** and **P3** systems**.**

	Conc. (M)	E_{corr} (mV vs SCE)	$-b_c$ (mV dec^{-1})	b_a (mV dec^{-1})	i_{corr} (mA cm^{-2})	EI_{icorr} (%)	C_R (mmY^{-1})	Rp (Ω cm^2)	EI_{Rp} (%)
	Blank	-445	199	194	5.22	----	60.39	8.17	----
	1×10^{-6}	-468	214	210	3.57	**31.6**	41.62	12.89	**36.6**
	1×10^{-5}	-463	194	188	2.45	**52.9**	28.57	16.92	**51.7**
P1	1×10^{-4}	-494	87	94	0.71	**86.4**	8.28	27.63	**70.0**
	2×10^{-4}	-457	99	96	0.07	**98.6**	0.82	302.39	**97.3**
	5×10^{-6}	-510	192	162	3.62	**30.6**	42.21	10.56	**22.63**
	1×10^{-5}	-516	183	155	2.81	**46.2**	32.76	12.97	**37.0**
P2	1×10^{-4}	-497	158	125	1.30	**75.1**	15.16	23.31	**64.9**
	2×10^{-4}	-488	117	97	0.30	**94.2**	3.50	76.76	**89.4**
	5×10^{-6}	-511	178	145	3.65	**30.0**	42.56	9.50	**26.6**
	1×10^{-5}	-510	165	135	1.95	**62.6**	22.73	16.53	**50.6**
P3	1×10^{-4}	-498	152	128	1.38	**73.6**	16.09	21.86	**62.6**
	2×10^{-4}	-495	115	108	0.61	**88.3**	7.11	39.64	**79.4**

An overview in Table 7, it is clearly stated that the i_{corr} values of carbon steel after the addition of **P1**, **P2** and **P3** are lower than those of white d, which is explained by better and strong adsorption of the latter on the steel surface. This decrease is proportional to the increase in the concentration and reaches a minimum value at 2×10^{-4} M. Consequently, the inhibitory efficiencies vary in the opposite direction and reach a maximum value of 98.4% for **P1**, 96.5% for **P2** and 90.1% for **P3**. It is also noted that the addition of **P1**, **P2** and **P3** had a clear effect on the values of b_c and b_a, indicating that the addition of these molecules involves a modification of the mechanism of the cathodic and anodic reactions. This same phenomenon has been noticed by several researchers and in different environments (sulfuric, hydrochloric, phosphoric, perchloric acid) [42-45].

It is evident that the corrosion inhibitors act by adsorption on the metal blocking the active sites, and the result will be the reduction of the anodic reaction and also retards the reaction of evolution of cathodic hydrogen. It should be noted here that the inhibitors treated in this study

come within this context and exhibit a mixed type inhibitory effect. Moreover, it is clear that the addition of the latter causes a slight displacement of the corrosion potential (E_{corr}) towards cathodic values. According to the literature, if the displacement of the corrosion potential in presence of the inhibitor relative to that of the acid alone is less than $\pm$ 85 mV, the inhibitor can be considered to be of mixed type [13,46-48].

The values of corrosion rate obtained from Eq. 6 (Table 7). The corrosion rate values decreased in the same trend by the presence of inhibitors as from other methods.

### 3.3 Electrochemical Impedance Spectroscopy measures

Among the most effective analytical tools for the behavior of the inhibitor on the metal surface is electrochemical impedance spectroscopy. The particularity of the latter is that it does not disturb the double layer of the metal solution interface. The Nyquist diagrams of the acid solution in the presence in the absence of inhibitor **P1, P2** and **P3** are shown in Figures 3a, 3b and 3c. This diagrams show a single semicircle capacitive loop at all studied concentrations of inhibitors. The increase in the concentration of inhibitors causes an increase in the diameter of the capacitive loops, indicating that the corrosion of carbon steel is managed by a load transfer process. In addition, we clearly notice that the capacitive loops are flattened towards the real axis, this phenomenon is mainly related to the roughness, the irregularity and the frequency dispersion effect of metal electrode surface.
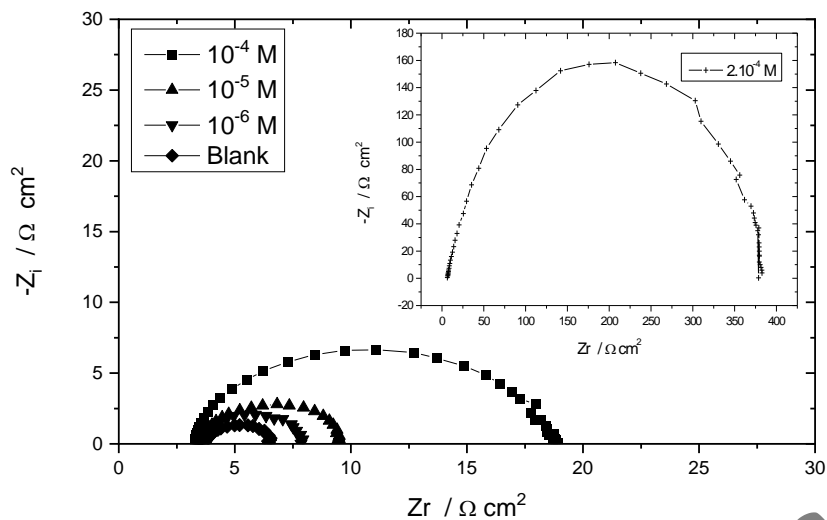
Fig. 3. EIS diagrams of carbon steel immersed in diverse amounts **P1** at 303 K.
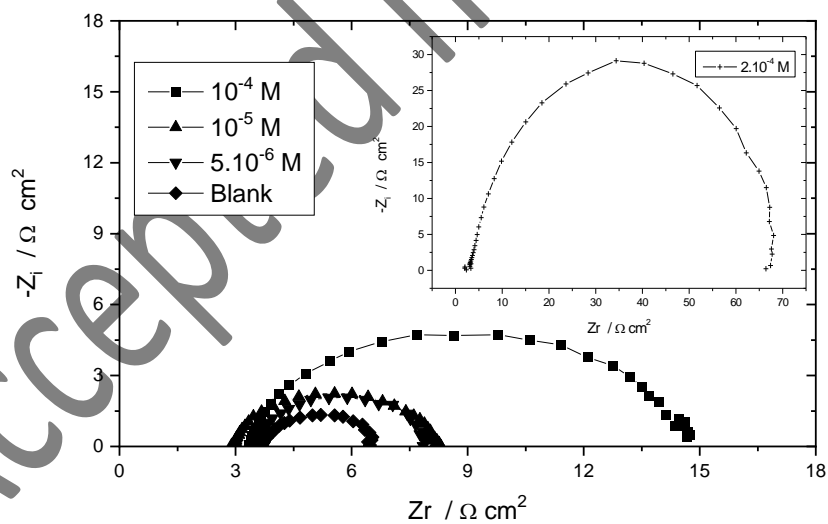

Fig. 3. EIS diagrams of carbon steel immersed in diverse amounts **P2** at 303 K.
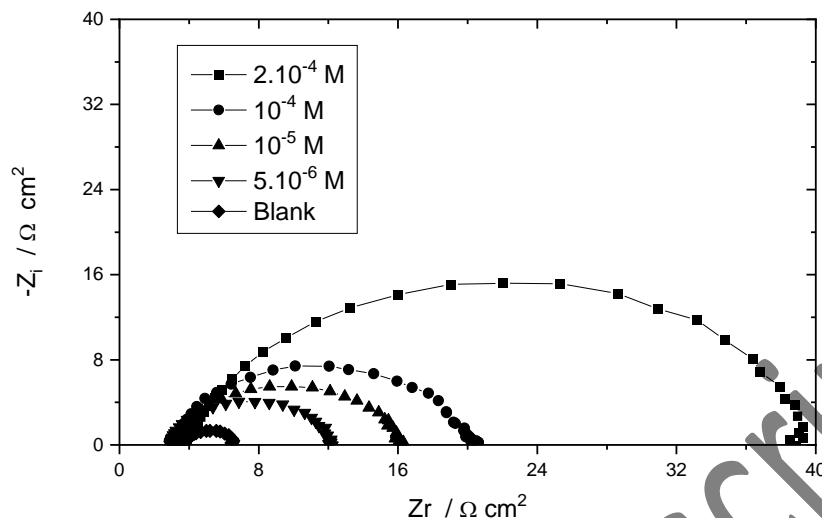
Fig. 3. EIS diagrams of carbon steel immersed in diverse amounts **P3** at 303 K.

So in this case a constant phase element (*CPE*) replaces the double layer capacitance (*C_{dl}*) because the perfect double layer is not formed. The experimentally obtained Nyquist diagram were fitter by a simple Randel circuit (Fig. 4) formed of a solution resistance (R_s), a CPE and a polarization (R_p). The parameters taken from the impedance spectra (the charge transfer resistance R_t, n values, the CPE (*Q*) values, the double layer capacitance C_{dl} and inhibition efficiency) are given are presented in Table 8.

Ddetailed method of calculating *C_{dl}* values from *CPE* values is identical to that given in our previous work [23].
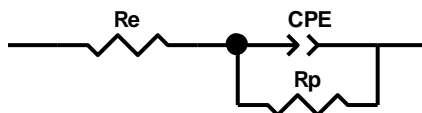
Fig. 4. Schematic representation of the equivalent electrical circuit used to model the inhibited or uninhibited carbon steel-acid medium interface.

17

Table 8

EIS for carbon steel /0.5 M H_2SO_4 with **P1**, **P2** and **P3** systems**.**

	Conc. (M)	R_p ($\Omega\, cm^2$)	Q ($\Omega^{-1}.cm^{-2}.\,s^n$)	*n*	C_{dl} ($\mu F\, cm^{-2}$)	EI_{Rp} (%)
	Blank	2.77	3.44×10^{-4}	0.86	397	----
P1	1×10^{-6}	4.30	7.43×10^{-4}	0.87	315	35.6
	1×10^{-5}	5.85	4.38×10^{-4}	0.90	226	52.6
	1×10^{-4}	14.76	1.57×10^{-4}	0.89	187	81.2
	2×10^{-4}	348.7	3.31×10^{-5}	0.88	18	99.2
P2	5×10^{-6}	4.30	4.68×10^{-4}	0.94	315	35.6
	1×10^{-5}	4.98	5.46×10^{-4}	0.90	283	44.4
	1×10^{-4}	10.65	4.16×10^{-4}	0.90	228	74.0
	2×10^{-4}	60.93	1.44×10^{-4}	0.86	67	95.4
P3	5×10^{-6}	8.87	4.13×10^{-4}	0.95	308	34.7
	1×10^{-5}	12.21	5.10×10^{-4}	0.90	290	52.6
	1×10^{-4}	16.35	3.38×10^{-4}	0.92	215	64.6
	2×10^{-4}	33.08	1.84×10^{-4}	0.92	118	82.5

From Table 8, it should be mentioned that an increase in the amount of the compounds in question is accompanied by a growth in the values of R_p, on the other hand the values of C_{dl} vary in the opposite sens. This decrease in C_{dl} is proportional to the increase in the thickness of the electric double layer, which proves the adsorption process of these compounds (**P1**, **P2** and **P3**) on the metal surface. Besides, an increase in R_p confirms the formation of a barrier film at the metal / solution interface. On the other hand, for the three compounds, n reaches approximately in the same value. This result can be interpreted as an indication of the degree of heterogeneity of the metal surface, corresponding to a small depression of the double layer capacitance semicircle [49].

Finally, it should be noted that these results confirm those who abstained from the method of mass loss and polarization curves.
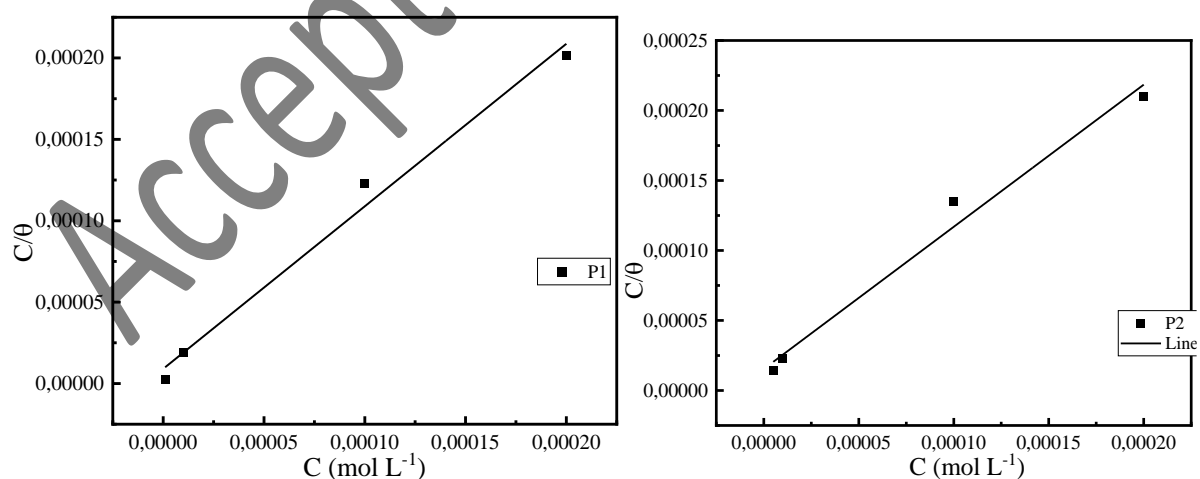
3.4. Adsorption isotherm

The literature study has shown that in an acidic environment, the corrosion inhibition of metals by organic compounds is generally explained by their adsorption [50-54]. The latter can be classified into two large families according to the nature of the interactions which "retain" an adsorbate given on the surface of an adsorbent: physical adsorption and chemical adsorption which involve respectively weak or strong bonds between chemical species adsorbed and adsorbent. The laws of variation which relate, at a given temperature, the concentration of adsorbate (in the occurrence of the inhibitor) in a given medium to the amount of this adsorbate adsorbed on a solid adsorbent (steel) in equilibrium with this medium can be described by equations called adsorption isotherms; the objective being to correlate the adsorption isotherms with thermodynamic properties characteristic of the adsorbate-adsorbent pair.
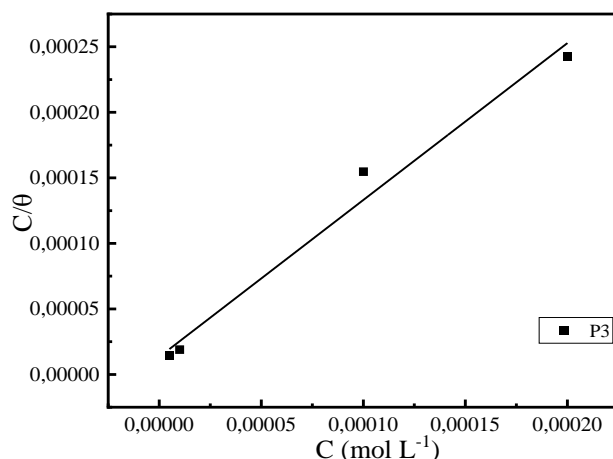
The best fit of the results was made by the Langmuir isothermal adsorption equation [55-57]:

$$\frac{C}{\theta} = \frac{1}{K_{ads}} + C \tag{8}$$

where C is the concentration of inhibitor, K_{ads} is the adsorptive equilibrium constant.

Plots of C/θ against C yield straight lines as shown in Fig. 5.

Fig. 5. Langmuir adsorption isotherm of inhibitors in 0.5 M H_2SO_4 at 303 K.

Both linear correlation coefficient (R > 0.975) and slope are very close to 1, indicating the adsorption of **P1**, **P2** and **P3** on carbon steel surface obeys the Langmuir adsorption isotherm. Among the hypotheses of the application of this isotherm is that the adsorbed molecule occupies only one site and that there is no interaction between the molecules [58-59]. In addition, a high value of the K_{ads} equilibrium constant reflects a high capacity and spontaneous adsorption of these molecules on the metal surface.

In addition, the $\Delta G^{°}_{ads}$ can be calculated from the values of the adsorption constants using equation:

$$\Delta G^{°}_{ads} = -RT \times Ln[55.5 \times K_{ads}] \tag{9}$$

The values of K_{ads} and $\Delta G^{°}_{ads}$ are listed in Table 9.

Negative values of $\Delta G^{°}_{ads}$ indicate that the phenomenon of adsorption of molecules on the steel surface is a spontaneous process. Generally, values of $\Delta G^{°}_{ads}$ up to -20 kJ/mol correspond to electrostatic interactions (a physical adsorption) between the metal and the inhibitory molecules while those more negative than -40 kJ/mol involve the formation of coordination bonds between molecules and the metal surface (chemisorption) [60-61]. On the other hand, the values of the standard free energy of adsorption are situated between these two values, resulting in the contribution of the two types of adsorption [62]. According to the

20

values obtained for ΔG_{ads}°, we can say that the adsorption phenomenon in this case is provided by mixed adsorption (both chemical and physical) with a tendency to chemical adsorption.
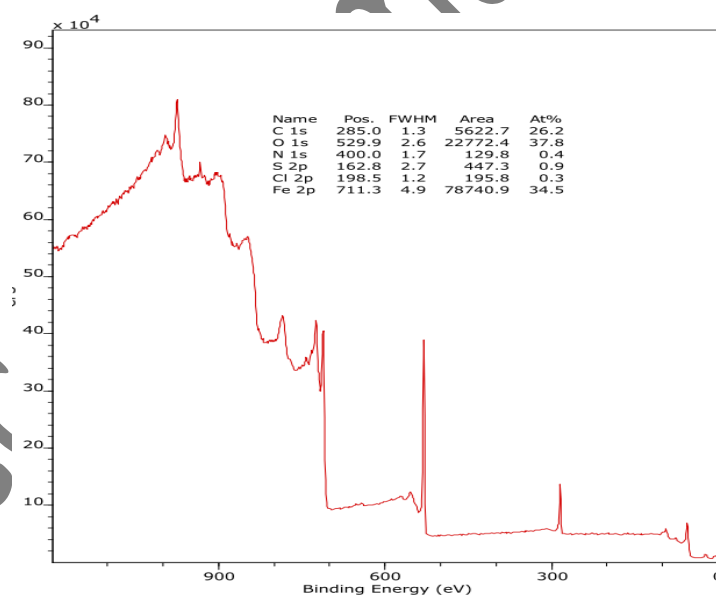
Table 9.

Thermodynamic parameters for the studied systems.

| Inhibitors	K_{ads} (M^{-1})	Slope	ΔG_{ads}° (kJ/mol)
P1	1.11×10^5	0.998	-39.38
P2	6.49×10^4	1.010	-38.03
P3	5.69×10^3	1.040	-31.90

3.5 X-ray photoelectron spectroscopy

The XPS analysis of carbon steel immersed in 0.5 M H_2SO_4 in presence of **P1** (2×10^{-4} M) for 24 h at 303 K is shown in Fig. 6.


Fig. 6. Survey spectra of XPS analysis for the system: carbon steel/0.5 M H_2SO_4 + 2×10^{-4} M of **P1.**

It contains C, O, N, S, Fe and adventurous contaminates such as Cl. The spectrum of the C 1s peak is shown in Fig. 7. Three peaks are evident independently of the microstructure. The first component at 286.4 eV is related to the carbon atoms bonded (nitrogen in C=N and C–N bonds in the thiazole ring and sulfur in C–S bond); the second component at a BE 285.0 eV is due to the C–C, C=C and C–H. The third peak situated approximately at 289 eV) is ascribed to the carbon atom of the $C=N^+$ in the tiazole ring [30, 63-64].
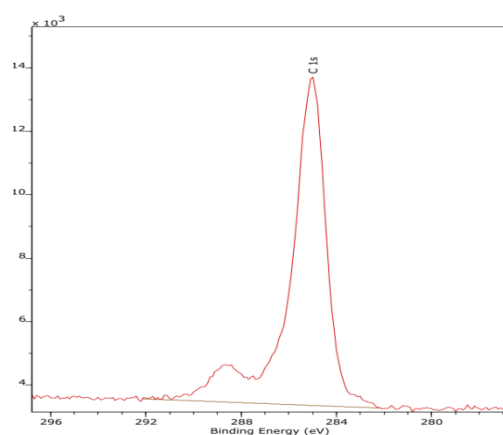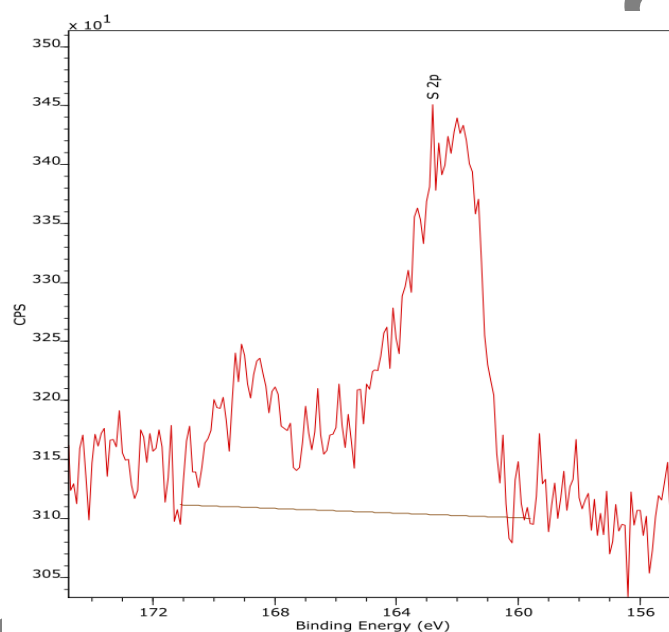

Fig. 7. High resolution C 1s spectra of XPS analysis.

The XPS spectra of O 1s (Figure 8) present three distinct peaks, the first one at 529.6 eV attributed the oxide bond (MO), the second peak at the 531.1 eV is due to metal hydroxide (MOH) and the third peak at of 532.8 eV is due to metal water bonds (MH_2O) [65].
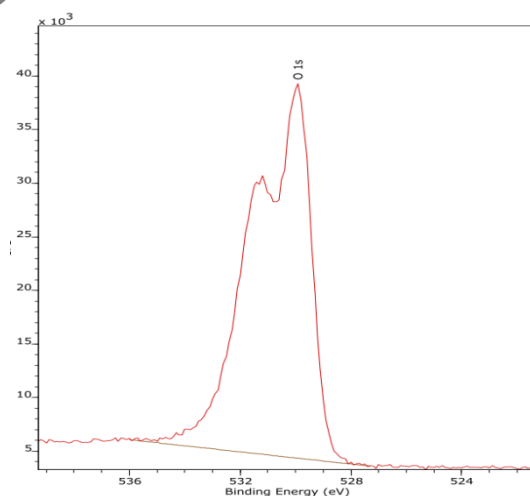
Fig. 8. High resolution O 1s spectra of XPS analysis.

The S 2p spectrum shows two main peak, the first one located around at 163–164 eV (Figure 9). This peak can be attributed to the C–S–C and to C= S structure in the thiazole ring [66-67]. The second of bending energy at 169-170 is attributed to the characteristic peak of SO_4^{2-} [68]. Globally, from the spectrum S 2p we can say that the presence sulfur is of low quantity on the metal surface.

Fig. 9. High resolution S 2p spectra of XPS analysis.

The N 1s spectrum of protected carbon steel with **P1** in 0.5 M H_2SO_4, given in Figure 10, shows one main peak (399–400 eV). From the literature, this peak is attributed to the $-N <$ (in the thiazole) [69]. The same remark of the presence of a small quantity of sulfur on the surface was noticed for the case of the nitrogen atom.
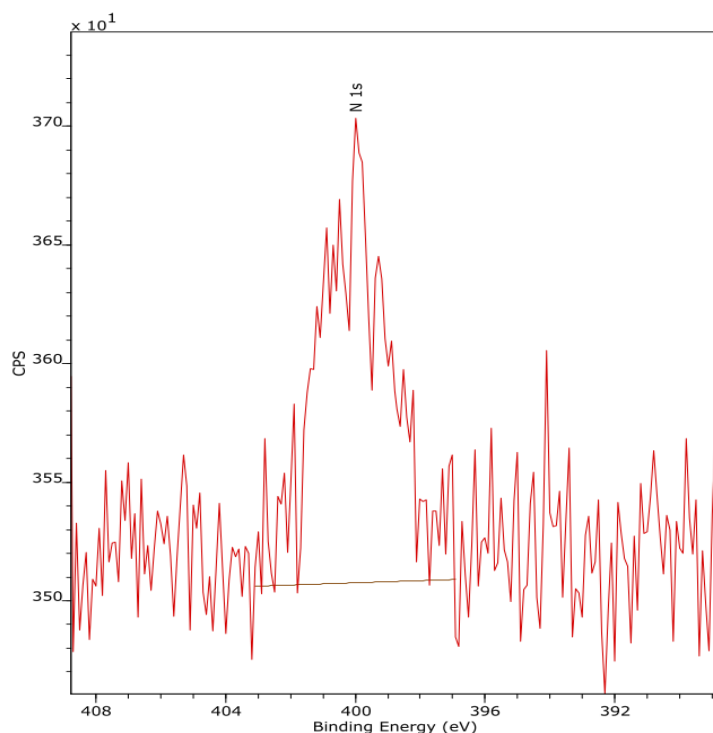
Fig. 10. High resolution N 1s spectra of XPS analysis.

For the spectrum of Fe 2p (Fig. 11) in the presence of the product **P1**, there is the presence of a doublet: 712 eV (Fe 2p1/2) and 725 eV (Fe 2p3/2), which confirms the oxidation of the surface of carbon steel [70-71]. Also, two little peaks, the first one at 707 eV characteristic of Fe^0 and the second one appears at 719 eV (Fe(III)) [66]. The peak at 712.56 eV represents the ferric ion of ferric oxide (Fe_2O_3) and ferric oxyhydroxide (FeOOH) [72].
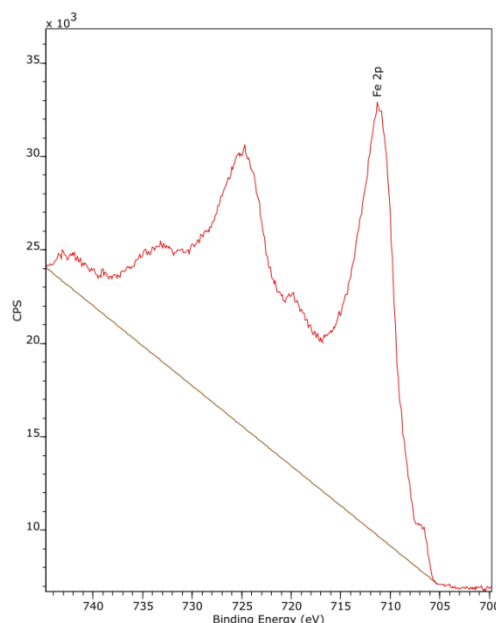
Fig. 11. High resolution Fe 2p1/2 and Fe 2p3/2 spectra of XPS analysis.

3.6 Computational results via DFT reactivity

The use of organic molecules as inhibitors against the corrosion process in an aggressive medium allowed us to investigate purely theoretical approaches to explain the nature of action of these inhibitors on the metal surface under study [73]. Among these most widely used approaches, we note the DFT method and molecular dynamics simulation (MDS) [74]. The DFT method focuses on chemical reactivity issues such as electronic behavior at the molecular structure level, while MDS investigates interatomic interactions at the inhibitor/metal interface. Fig. 12 illustrates the optimized structures, the electron density distributions of HOMO and LUMO. The computational results reveal that the special configuration of the optimized molecules **P1**, **P2**, **P3**, and **TS1** do not indicate any negative frequencies, which explains that the spatial representation of these molecules is more stable.

The distribution of the frontier molecular orbitals (HOMO and LUMO) on the skeleton of the considered molecules is detailed in Fig. 12. The evaluation of this figure suggests that the electron density of HOMO and LUMO is repatriated over the entire molecular structure of **P1**, **P2**, **P3**, and **TS1**. This result shows that these molecules have several active centers spread

25

over the entire molecular surface. Therefore, this performance may lead to parallel adsorption of species on the metal surface of interest. In this case, it is obvious that these derivatives adsorb strongly on the metal support in order to reduce the corrosion phenomenon in H_2SO_4.

Optimized structure	HOMO	LUMO
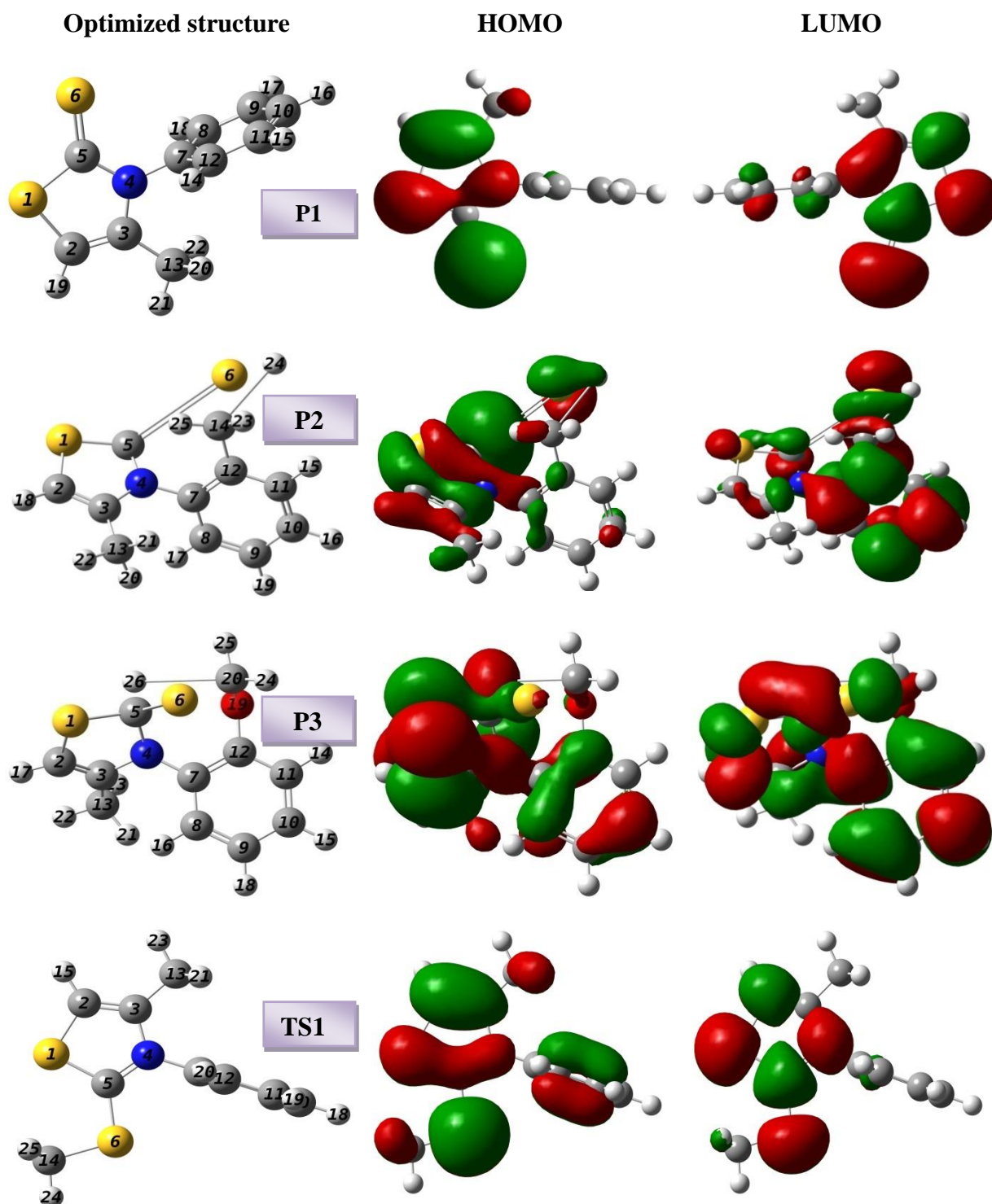
Fig .12. Optimized structures, the electron density distributions of HOMO and LUMO of **P1**, **P2**, **P3**, and **TS1**.

The global descriptors surveyed in this novel research are summarized in Table 10. It is well known that the HOMO energy (E_{HOMO}) is associated with the power of molecules to contribute electrons. On the other hand, the LUMO energy (E_{LUMO}) is directly proportionate to the capability of molecules to receive electrons [75]. The values gathered in Table 10 demonstrate that the **P1** molecule classifies as the first and most electron donating inhibitor at the vacant orbitals located in the iron surface in comparison with the other derivatives evaluated. Conversely, the electron acceptor capacity of this molecule is lower than the other optimized compounds. The reactivity of an organic molecule can be assessed by the value of the energy gap (ΔE_{gap}) [76]. It is widely agreed that the small value of ΔE_{gap} of this molecule indicates a high chemical reactivity, hence a very high anti-corrosion property [77]. The ΔE_{gap} values listed in Table 10 are ordered as follows: **P1< ST1 < P2< P3**. Thus, their corrosion inhibition efficiency displays an inverse trend, consistent with the experimental results. The number of transferred electrons (ΔN_{110}) is another parameter that allows us to evaluate the power of an organic molecule to release electrons [71]. It is recognized that the positive value of this descriptor indicates an electron donating capacity and vice versa as this. The degree of ΔN_{110} of the selected molecules is given as follows: **P1 > ST1 > P2>P3**. The high inhibitory power of **P1** due to its strong donor-acceptor interactions with iron atoms can be supported by the low values of the global electronegativity ($\chi = 3.077$ eV) and the global hardness ($\eta = 2.288$ eV) [78].

Table 10

DFT-descriptors describing the reactivity of **P1, P2, P3**, and **TS1.**

Quantum descriptors	**P1**	**P2**	**P3**	**ST1**
E_{HOMO} (eV)	-5.366	-5.847	-5.971	-10.340
E_{LUMO} (eV)	-0.789	-0.620	-0.381	-5.523
ΔE_{gap} (eV)	4.577	5.227	5.590	4.817
χ (eV)	3.077	3.233	3.176	7.931
η (eV)	2.288	2.613	2.795	2.408
ΔN_{110}	0.381	0.304	0.294	-0.646

It is recognized that the adsorption of an inhibitor compound onto a test metal surface is generally via active sites that are electron donors and acceptors. The more these sites are distributed throughout the molecular structure, the more protection there is for the attacking surface against corrosive species [79]. In our present analysis, the local selectivity (active sites) of **P1, P2, P3,** and **TS1** was determined using Fukui functions and molecular electrostatic potential (MEP).

The Fukui indices are obtained via GGA/PBE under the DNP (4.4) basis set using the DMol^3 module in Materials Studio ^{2016} as used by Rbaa et al. [80]. On the other hand, the regions of local reactivity were also mapped by the molecular electrostatic potential (MEP) using the Materials studio software. MEP is a very relevant approach to the analysis of regions or sites of electrophilic and nucleophilic attacks as well as hydrogen bonding interactions. Fig. 13 shows the MEP distribution on the structure of the optimized compounds. In this figure, it is evident that the red (negative) and blue (positive) regions indicate the nucleophilic and electrophilic reactivity of the species tested, respectively. Furthermore, the visual analysis of the images in the figure for the **P1**, **P2**, and **P3** reveals that the sulphur atoms (S1 and S6) carry a higher total density of MEPs (red color), which explains why these two heteroatoms behave as electron donor sites. On the other hand, the topological aspect of the cationic form of **TS1** molecule shows just the blue color, which means that this molecule has a receptor property for electrons arriving from occupied orbitals located in the metal surface.
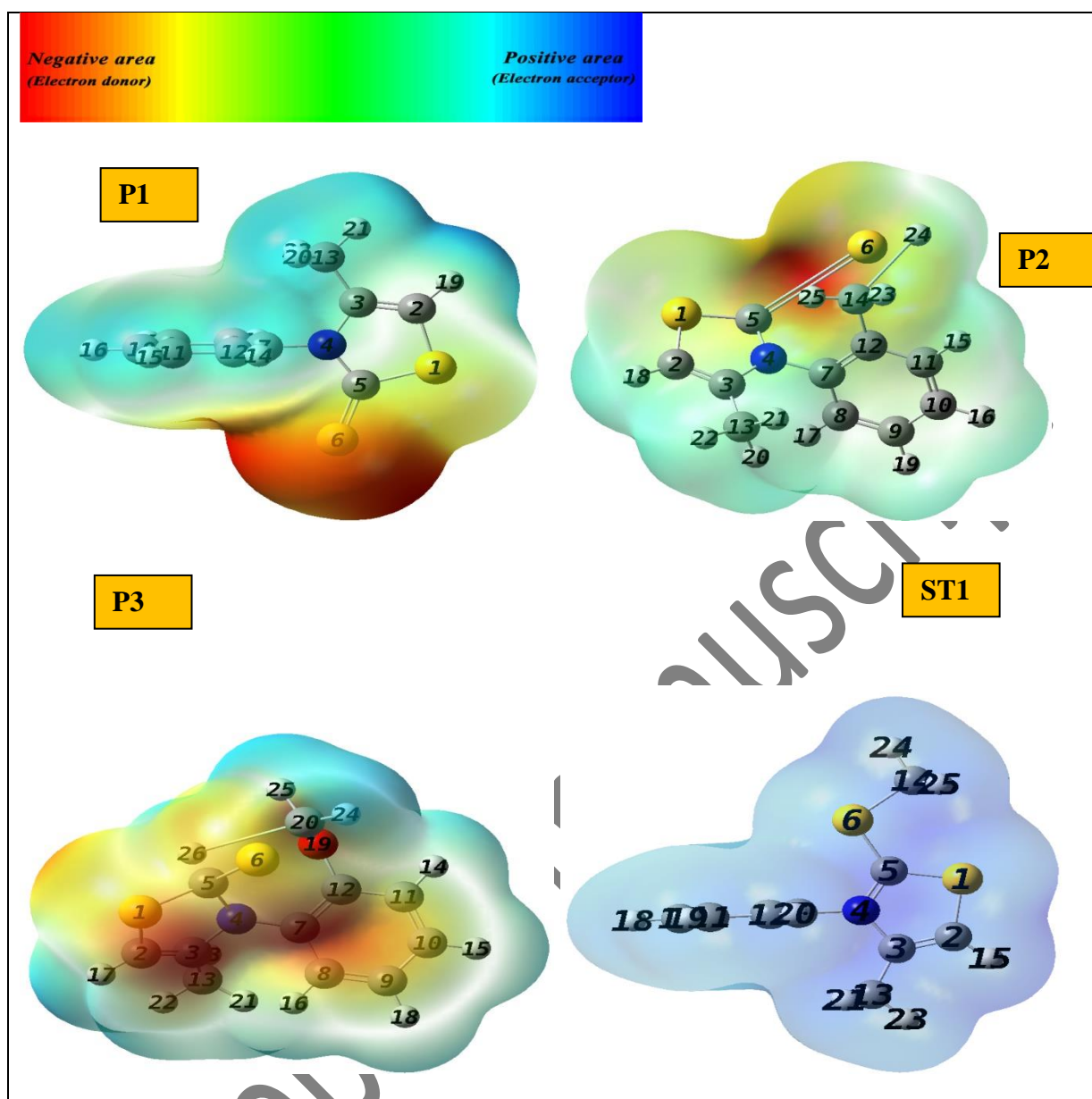
Fig. 13. MEP representation for **P1, P2, P3** and **TS1**.

Fukui functions allow describing the reactive sites that are responsible on the electrophilic (f_i^-) and nucleophilic (f_i^+) attacks of the molecules under review. Generally, the most condensed functions show the most active sites (atoms) [81]. The Fukui indices, which represent the local reactivity, are listed in Table 11. The data in the table shows that the sulphur heteroatoms S1 and S6 for **P1, P2, P3** and **ST1** are the electrophilic (f_i^-) attack sites that are able to share their electrons with the nucleophilic (f_i^+) centers in the iron surface. This effect can lead to the formation of covalent bonds that strengthen the adsorbed layer

against the corrosion process. Alternatively, the nucleophilic attack sites (electron attractors) for **P1, P2, P3** and **TS1** are represented by the atoms C5 and C10. These centers can receive electrons from the centers occupied in the iron surface. This behavior is due to the cationic form of **TS1**. For compound **TS1**, no electron-donor centers are seen, while several sites are observed to behave as electron-acceptor centers.

Table 11

Active sites revealed by the Fukui indices approach for **TO1, TO4, TO6** and **TS1**.

Atoms	TO1		TO4		TO6		ST1	
	f_i^-	f_i^+	f_i^-	f_i^+	f_i^-	f_i^+	f_i^-	f_i^+
S (1)	0.130	0.141	0.136	0.139	0.129	0.122	0.035	0.052
C (2)	0.071	0.042	0.066	0.043	0.052	0.038	0.054	0.080
C (3)	0.047	0.025	0.049	0.024	0.042	0.020	0.043	0.050
N (4)	0.036	0.027	0.035	0.027	0.028	0.019	0.027	0.036
C (5)	0.024	0.089	0.023	0.085	0.027	0.071	0.020	0.069
S (6)	0.295	0.190	0.292	0.188	0.310	0.180	0.045	0.050
C (7)	0.003	0.027	0.001	0.019	-0.003	0.030	0.033	0.012
C (8)	0.026	0.041	0.023	0.042	0.024	0.049	0.031	0.023
C (9)	0.039	0.043	0.034	0.039	0.035	0.041	0.037	0.037
C (10)	0.050	0.070	0.047	0.065	0.046	0.072	0.070	0.063
C (11)	0.033	0.042	0.026	0.042	0.027	0.049	0.048	0.039
C (12)	0.019	0.031	0.006	0.018	0.004	0.022	0.030	0.034
C (13)	0.017	0.014	0.017	0.013	0.016	0.013	0.018	0.016
C (14)	---	---	0.014	0.013	---	---	0.028	0.022
O (19)	---	---	---	---	0.029	0.020	---	---
C (20)	---	---	---	---	0.012	0.012	---	---

3.7 Molecular simulation

Interatomic interactions occurred at the metal/inhibitor interface are investigated using theoretical approaches such as molecular dynamics simulation as a method used more frequently in recent years [82-83]. In this section, the interaction performance between the target species and the simulated iron surface is illustrated in Fig.14 under the temperature of

303 K. The configurations represented in this figure show that the Tested molecules will adsorb by all their molecular structures on the first layer of the iron atoms. This quality indicates that the inhibitor molecules studied form a protective barrier against the corrosion process. This reveals that these inhibitory species carry several active sites spread across the molecular surface of the selected compounds.
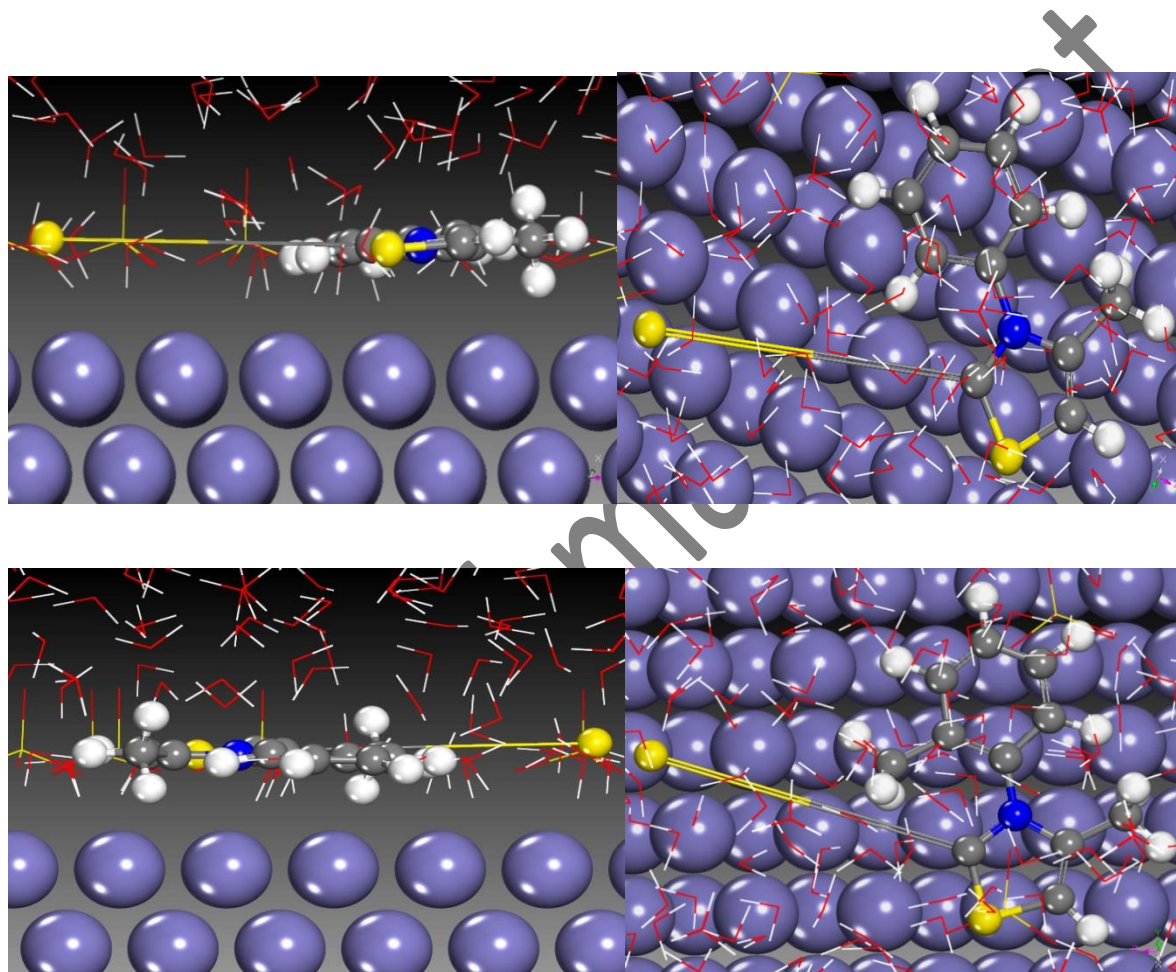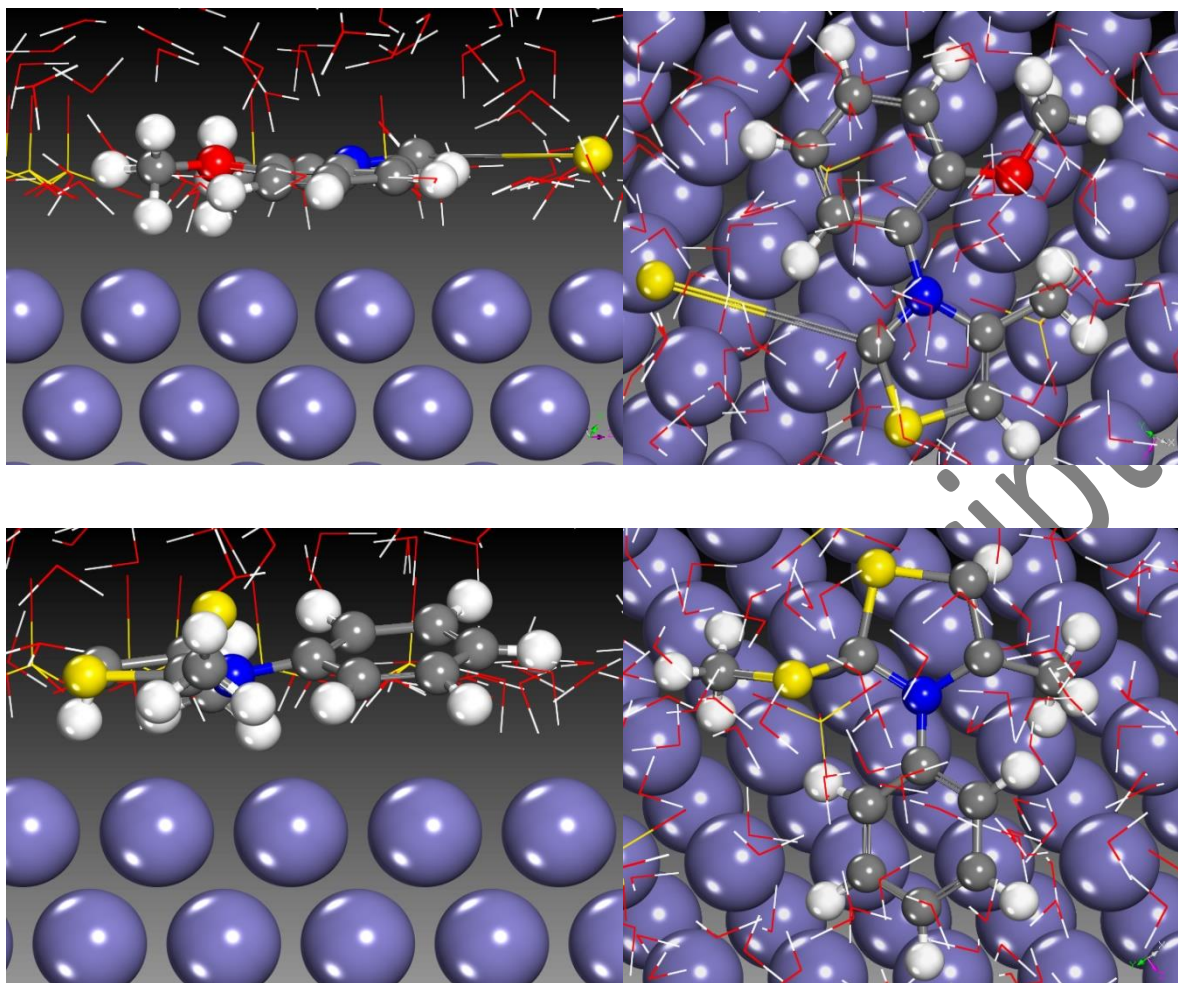
Fig. 14. Geometric configurations of adsorption of studied compounds onto iron.

Based on the most reasonable and stable adsorption configurations displayed in Fig. 14, the molecular dynamics method was used to calculate the values of different interaction and binding energies of **P1, P2, P3** and **TS1** on the simulated iron. The interaction energy ($E_{interaction}$) and binding energy ($E_{binding}$) between studied molecules and Fe (110) is calculated by Eqs.8 and 9 [84]:

$$E_{interaction} = E_{total} - (E_{surface+solution} + E_{inhibitor})$$

(8)

$$E_{binding} = -E_{interaction}$$

(9)

The results of the whole molecular simulation show that the values of $E_{interaction}$ for **P1, P2, P3** and **TS1** in relation to the adsorption surface are -128.340, -110.954, -100.434 and

32

-119.458 kJ/mol. These results imply that the adsorption procedure by the tested inhibitor molecules occurs spontaneously [85]. In contrast, the lower values of $E_{binding}$ can be due to the aggressiveness of the study medium such as H_2SO_4. A high value of $E_{bindind}$ shows that an inhibitor molecule adsorbs strongly to the metal surface. The adsorption intensity of the selected components is ranked in the following order: **P1 > TS1 > P2 > P3**. This order is in reasonable agreement with the order of inhibitory efficacy obtained experimentally.

The degree of corrosion resistance of the metal surface depends on the adsorbed molecules. This adsorption may also be influenced by the bonds that are conducted, which may be of a chemical or physical nature or both [86]. In general, if the value of a bond length in the range of 1-3.5 Å, so, the adsorption is controlled by chemisorption [87]. If this value is excluded from the range, so, there is chemisorption. In the present analysis, Fig.14 reveals that all the values appearing in the first peak at the inhibitor/metal interface are within the chemisorption interval except the Fe-N6 value of **TS1**. The chemical adsorption of the simulated compounds onto the first layer of iron atoms indicated that these compounds successfully inhibited the degradation of the investigated steel.
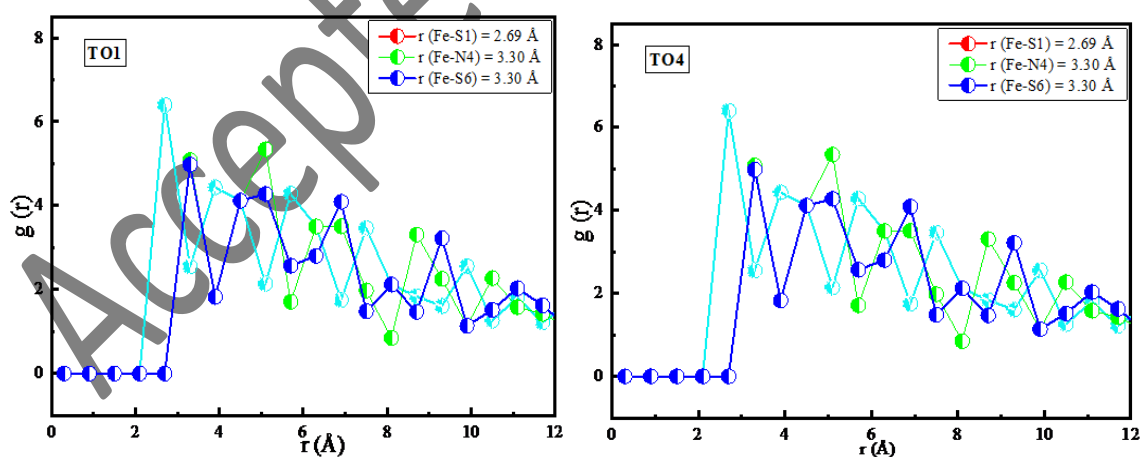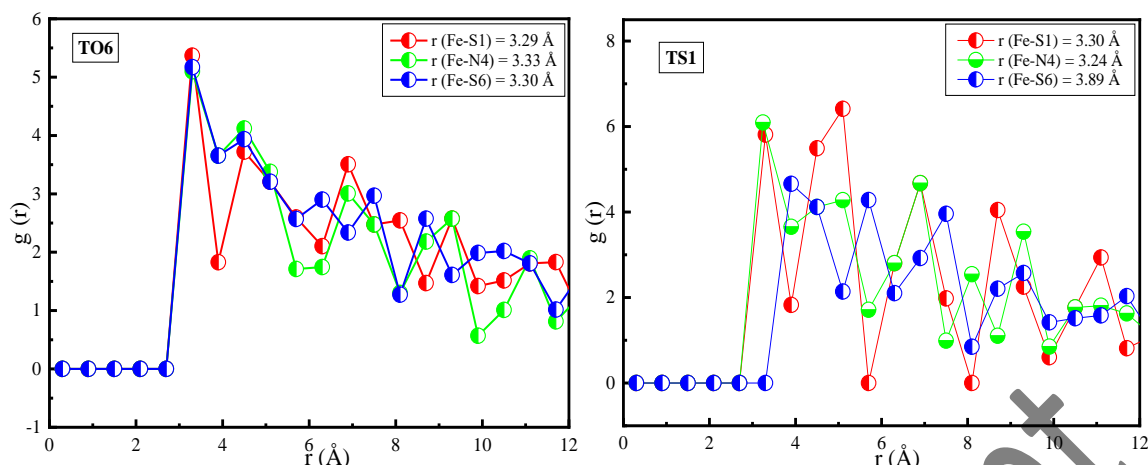
Fig. 14. RDF of **P1**, **P2**, **P3**, and **TS1** on iron at 303 K.

4. Conclusion

Three thiazole derivatives were tested as corrosion inhibitors for carbon steel in H_2SO_4 solution in this study. Weight loss, electrochemical, and XPS investigations were used to characterize the performance of inhibitors in depth. In addition, using DFT and MD simulations, the interactions between inhibitor molecules and carbon steel were investigated theoretically. The three inhibitors were found to be highly efficient against carbon steel corrosion in H_2SO_4, with P1 inhibitor having the best inhibition performance. Investigated inhibitors inhibited both anodic and cathodic corrosion processes, according to electrochemical studies. The Langmuir isotherm model is used to explain the adsorption of the three inhibitors on the steel surface. The XPS analysis revealed that the inhibitor compounds adsorb in a mixture of ways (physisorption and/or chemisorption). DFT calculations and MD simulation allowed us a good understanding between the anticorrosive activity and the chemical structure properties of these three inhibitors. This research demonstrated that this class of chemical compounds (thiazole derivatives) can be effective corrosion inhibitors and emphasized the need for further variants to be developed.

34

References

[1] A. Kumar Singh, B. Chugh, S. Thakur, B. Pani, H. Lgaz, I. Chung, S Pal, R. Prakash, Coll. Surf. A: Physicochem. Eng. Aspects 599 (2020) 124824.

[2] A. Kumar Singh, B. Chugh, M. Singh, S. Thakur, B. Pani, L. Guo, S. Kaya, G. Serdaroglu, J. Mol. Liq. 330 (2021) 115605.

[3] B. Chugh, S. Thakur, B. Pani, M. Murmu, P. Banerjee, A. Al-Mohaimeed, E.E. Ebenso, M. Singh, J. Singh, A. Kumar Singh, J. Mol. Liq. 330 (2021) 115649.

[4] B. Chugh, K. Singh, D. Poddar, S. Thakur, B. Pani, P. Jain, Carbohydrate Polymers 234, (2020) 115945.

[5] A. K. Singh, S. Thakur, B. Pani, G. Singh, New J. Chem. 42 (2018) 2113-2124.

[6] B. Chugh, A. K. Singh, S. Thakur, B. Pani, A. K. Pandey, H. Lgaz, I. M. Chung, E. E. Ebenso, J. Phys. Chem. C 123 (37) (2019) 22897–22917.

[7] A. K. Singh, M. A. Quraishi, Corros. Sci. 52(2010) 1373-1385.

[8] A. K.Singh, M. A. Quraishi, Corros. Sci. 52 (2010) 152-160.

[9] M.A. Quraishi, D.S. Chauhan, V.S. Saji, Heterocyclic Organic Corrosion Inhibitors: Principles and Applications. 1st Edition. Elsevier Inc. Amsterdam (2020) 1-19.

[10] X. Zuo, W. Li, W. Luo, X. Zhang, Y. Qiang, J. Zhang, , B. Tan, J. Mol. Liq. 321 (2021) 114914.

[11] B. Tan, J. He, S. Zhang, C. Xu, S. Chen, H. Liu, W. Li, J. Coll. Interf. Sci. 585 (2021) 287-301.

[12] B. Tan, S. Zhang, H. Liu, Y.Guo, Y.Qiang, W Li, L. Guo, C. Xu, S. Chen, J. Coll. Interf. Sci. 538 (2019) 519-529.

35

[13] M. Zebida, O. Benali, U. Maschke, M. Trainsel, Inter. J. Corros. Scale Inhib. 8(3) (2019) 613–627.

[14] H. B. Ouici, O. Benali, Y. Harek, L. Larabi, B. Hammouti, A. Guendouzi, Res. Chem. Intermed. 39 (2013) 2777–2793.

[15] H. B. Ouici, O. Benali, Y. Harek, L. Larabi, B. Hammouti, A. Guendouzi, Res. Chem. Intermed. 39 (2013) 3089–3103.

[16] A. Attou, M. Tourabi, A. Benikdes, O. Benali, H.B. Ouici, F. Benhiba, A. Zarrouk, C. Jama, F. Bentiss, Coll. Surf. A: Physicochem. Eng. Aspects 604 (2020) 125320.

[17] R. Morigi, B. Vitali, C. Prata, R. A. Palomino, A. Graziadio, A. Locatelli, M. Rambaldi, A. Leoni, Med. Chem. 14(3) (2018) 311-319.

[18] H. He, H. Jiang, Y. Chen, J. Ye, A. Wang, C. Wang, Nat. Commun. 9 (2018) 2550.

[19] K. Liaras, M. Fesatidou, A. Geronikaki, Molecules 23 (3) (2018) 685.

[20] M. Rezaei, H. T. Mohammadi, A. Mahdavi, M. Shourian, H. Ghafouri, Int. J. Bio. Macromol. 108 (2018) 205-213.

[21] J. Tomasi, B. Mennucci, R. Cammi, Chem. Rev. 105 (2005) 2999-3094.

[22] F. Benhiba, Y. ELaoufir, M. Belayachi, H. Zarrok, A. El Assyry, A. Zarrouk, B. Hammouti, E. E. Ebenso, A. Guenbour, S. S. Al Deyab, H. Oudda, J. Der Pharma. Lett. 6 (4) (2014) 306-318.

[23] E. Alibakhshi, M. Ramezanzadeh, G. Bahlakeh, B. Ramezanzadeh, M. Mahdavian, M. Motamedi, J. Mol. Liq. 255 (2018) 185 –198.

[24] F. Benhiba, Z. Benzekri, A. Guenbour, M. Tabyaoui, A. Bellaouchou, S. Boukhris, H. Oudda, I.Warad, A. Zarrouk, Chin. J. Chem. Eng. 28 (5) (2020) 1436-1458.

[25] J. Saranya, F. Benhiba, N. Anusuya, R. Subbiah, A. Zarrouk, S. Chitra, Coll. Surf A: Physico. Eng. Aspects 603 (2020) 125231.

[26] J.-P. Zeng, Y. Dai, W.-Y. Shi, J.-L. Shao, G.-X. Sun, Surf. Interf. Anal. 47 (2015) 896-902.

[27] H.C. Andersen, J. Chem. Phys. 72 (1980) 2384-2393.

[28] M. Finšgar, , Corros. Sci. 169 (2020) 108632.

[29] H. B. Ouici, M. Tourabi, O. Benali, C. Selles, M. Traisnel, C. Jama, F. Bentiss, R. Salghi, J. Mater. Environ. Sci. 7(8) (2016) 2971-2988.

[30] H. B. Ouici, M. Tourabi, O. Benali, C. Selles, C. Jama, A. Zerrouk, F. Bentiss, J. Electroanal. Chem. 803 (2017) 125-134.

[31] A. Benikdes, O. Benali, A. Tidjani, M. Tourabi, H. Ouici, F. Bentiss, J. Mater. Environ. Sci. 8(9) (2017) 3175-3183.

[32] H. B. Ouici, M. Belkhouda, O. Benali, R. Salghi, L. Bammou, A. Zarrouk, B. Hammouti, Res. Chem. Intermed. 41 (2015) 4617–4634.

[33] I. Danaee, M. Gholami, M. RashvandAvei, M.H. Maddahy, J. Ind. Eng. Chem. 26 (2015) 81-94.

[34] O. Radovici. In: Proceedings of the 2nd European Symposium on Corrosion Inhibitors. Ann. Univ. Ferrara (Italy). 1965, p. 178.

[35] A. Popova, E. Sokolova, S. Raicheva, M. Christov, Corros. Sci. 45(1) (2003) 33–58.

[36] A. Attou, A. Benikdess, O. Benali, H.B. Ouici, A. Guendouzi, Inter. J. Chem. Biochem. Sci. 17 (2020) 120-128.

[37] O. Benali, M. Zebida, U. Maschke, J. Ind. Chem. Soc.98 (8) (2021) 100113.

[38] S. Hejazi, Sh. Mohajernia, M.H. Moayed, A. Davoodi, M. Rahimizadeh, M. Momeni, A. Eslami, A. Shiri, A. Kosari, J. Indust. Eng. Chem. 25 (2015) 112–121.

[39] W. Gonga, B. Xu, X. Yin, Y. Liu, Y. Chen, W. Yang, J. Taiwan Instit. Chem. Engineers 97 (2019) 466–479.

[40] M. El Azhar, M. Traisnel, B. Mernari, L. Gengembre, F. Bentiss, M. Lagrenée, Appl. Surf. Sci. 185 (2002) 197–205.

[41] M. Lagrenée, B. Mernari, M. Bouanis, M. Traisnel, F. Bentiss, Corros. Sci. 44(3) (2002) 573-588.

[42] M. El Faydy, B. Lakhrissi, C. Jama, A. Zarrouk , L. O. Olasunkanmi, E.E. Ebenso, F. Bentiss, J. Mater. Res. Tech. 9 (1) (2020) 727-748.

[43] X. Li, S. Deng, G. Du, X. Xie, J. Taiwan Instit. Chem. Eng. 114 (2020) 263-283.

[44] F. Chaib ,·H. Allali, O. Benali, Guido Flamini, Inter. J. Chem. Biochem. Sci. 18 (2020) 129-136.

[45] E.E.Oguzie, Y. Li, F.H. Wang, J. Coll. Interf. Sci. 310 (1) (2007) 90–98.

[46] M. Behpour, S.M. Ghoreishi, N. Soltani, M. Salavati-Niasari, M. Hamadanian, A. Gandomi, Corros. Sci. 50(8) (2008) 2172–2181.

[47] L. Larabi, O. Benali, Y. Harek, Port. Electrochim. Acta 24 (2006) 337−346.

[48] S. Cheng, S. Chen, T. Liu, X. Chang, Y. Yinet, Mater. Lett. 61(14-15) (2007) 3276−3280.

[49] O. Benali, L. Larabi, S. M. Mekelleche, Y. Harek, J. Mater. Sci. 41 (2006) 7064–7073.

[50] S. Ramesh Kumar, I. Danaee, M. Rashvand Avei, M. Vijayan, J. Mol. Liq. 212 (2015) 168-186.

[51] I. Danaee, P. Nikparsa, J. Mater. Eng. Perf. 28 (2019) 5088-5103.

[52] I. Ahamad, R. Prasad, M.A. Quraishi, Corros. Sci. 52 (2010) 933.

[53] W.H. Li, Q. He, S.T. Zhang, C.L. Pei, B.R. Hou, J. Appl. Electrochem. 38 (2008) 289-295.

[54] H. Li, D. Dzombak, R. Vidic, Ind. Eng. Chem. Res. 51 (2012) 2821-2829.

[55] S. Deng, X. Li, H. Fu, Corros. Sci. 53 (2011) 822.

[56] M. Tourabi, K. Nohair, M. Traisnel, C. Jama, F. Bentiss, Corros. Sci. 75 (2013) 123–133.

[57] J.F. Watts, J. Wolstenholme, An Introduction to Surface Analysis by XPS and AES, John Wiley and Sons Inc., UK, 2003.

[58] X. Li, S. Deng, H. Fu, G. Mu, N. Zhao, Appl. Surf. Sci. 254 (2008) 5574–5586.

[59] F. Bentiss, M. Traisnel, L. Gengembre, Appl. Surf. Sci. 161 (2000), 194–202.

[60] E.T. Kang, K.G. Neoh, K.L. Tan, Phys. Rev. B 44 (1991) 10461–10469.

[61] C.D. Wagner, W.M. Riggs, L.E. Davis, J.F. Moulder, G.E. Muilenberg (Eds.), Handbook of X-ray Photoelectron Spectroscopy, Perkin Elmer Corporation (Physical Electronics), Eden Prairie, Minnesota, 1979, pp 190.

[62] F. Moulder, W.F. Stickle, P.E. Sobol and K.D. Bomben, Handbook of X-Ray Photoelectron Spectroscopy, Ed: J. Chastain, Perkin-Elmer Corp, Minnesota, USA, 1992.

[63] A. Singh , K.R. Ansari, D. Singh Chauhan , M.A. Quraishi, S. Kaya, Sust. Chem. Pharm. 16 (2020) 100257.

[64] Zhang, Z., Chen, S., Li, Y., Li, S., Wang, L., Corros. Sci. 51(2) (2009) 291–300.

[65] Bouanis, F., Bentiss, F., Traisnel, M., Jama, C., Electrochim. Acta 54 (2009) 2371–2378.

[66] Z. Rouifi, M. Rbaa, Ashraf S. Abousalem, F. Benhiba, T. Laabaissi, H. Oudda, B. Lakhrissi, A. Guenbour, I. Warad, A. Zarrouk, Surf. Interf. 18 (2020) 100442.

[67] F. ElHajjaji, M. Messali, A. Aljuhani, M.R. Aouad, B. Hammouti, M.E. Belghiti, M.A. Q uraishi, J. Mol. Liq. 249 (2018) 997-1008.

[68] N. Lotfi, F. Benhiba, N. Chahboun, H. Bourazmi , M. El Hezzat , A. H. Al Hamzi , H. Zarrok1, A. Guenbour, M. Ouhssine , H. Oudda, A. Zarrouk, Der Pharm. Lett. 7 (9) (2015) 1-7.

[69] G. Serdaroglu, S. Kaya, R. Touir , J. Mol. Liq. 319 (2020) 114108.

[70] Z.L. Seeger, E.I. Izgorodina, J. Chem. Theory Comput. 16 (10) (2020) 6735-6753.

[71] F.E. Awe, S.O. Idris, M. Abdulwahab, E.E. Oguzie, Cogent Chem. 1 (2015) 1112676.

[72] T. Laabaissi, F. Benhiba, Z. Rouifi, M. Missioui, K. Ourrak, H. Oudda, Y. Ramli, I. Warad, M. Allali, A. Zarrouk, Int. J. Corros. Scale Inhib. 8(2) (2019) 241–256.

[73] Z. Rouifi, M. Rbaa, Ashraf S. Abousalem, F. Benhiba, T. Laabaissi, H. Oudda, B. Lakhrissi, A. Guenbour, I. Warad, A. Zarrouk, Synthesis, Surf. Interf. 18 (2020) 100442.

[74]F. ElHajjaji, M. Messali, A. Aljuhani, M.R. Aouad, B. Hammouti, M.E. Belghiti, M.A. Quraishi, J. Mol. Liq. 249 (2018) 997-1008.

[75] N. Lotfi, F. Benhiba, N. Chahboun, H. Bourazmi , M. El Hezzat , A. H. Al Hamzi , H. Zarrok1, A. Guenbour, M. Ouhssine , H. Oudda, A. Zarrouk, Der Pharm. Lett. 7(9) (2015) 1-7.

[76] G. Serdaroglu, S. Kaya, R. Touir , J. Mol. Liq. 319 (2020) 114108.

[77] Z.L. Seeger, E.I. Izgorodina, J. Chem. Theory Comput. 16 (10) (2020) 6735-6753.

[78] T. Laabaissi, F. Benhiba, Z. Rouifi, M. Missioui, K. Ourrak, H. Oudda, Y. Ramli, I. Warad, M. Allali, A. Zarrouk, Int. J. Corros. Scale Inhib. 8(2) (2019) 241–256.

[79] A. Morgenstern, T.R. Wilson, M.E. Eberhart, J. Phys. Chem. A, 121 (2017) 4341-4351

[80] M.Rbaa, F. Benhiba, P. Dohare, L. Lakhrissi, R. Touir, B. Lakhrissi, A. Zarrouk, Y. Lakhrissi, Chem. Data Collect. 27(2020) 100394.

[81]   A.O. Zacharias, A. Verghese, K.B. Akshaya, M.S. Savitha, L. George,   J.   Mol. Struct. 1158 (2018)1-13.

[82] H. Rahmani, K.I. Alaoui , M. EL Azzouzi , F. Benhiba, A. El Hallaoui, Z. Rais, M. Taleb, A. Saady , B. Labriti , A. Aouniti, A. Zarrouk, Chem. Data Collect. 24 (2019) 100302.

[83] A. Elgendy, H. Nady, M. El-Rabiei, A.A. Elhenawy, RSC Adv. 9 (2019) 42120-42131.

[84] M. El Faydy, F. Benhiba, H. About, Y. Kerroum, A. Guenbour, B. Lakhrissi, I. Warad, C. Verma, El-S. M. Sherif, E. E. Ebenso, A. Zarrouk, J. Colloid Interface Sci. 576 (2020) 330–344.

[85] Z. Rouifi, M. Rbaa, F. Benhiba, T. Laabaissi, H. Oudda, B. Lakhrissi, A. Guenbour, I.Warad, A. Zarrouk , J. Mol. Liq. 307 (2020) 112923

[86] V. Mehmeti, F.I. Podvorica, Materials 11 (2018) 893.

[87] A. Saady, E. Ech-chihbi, F. El-Hajjaji, F. Benhiba, A. Zarrouk, Y. Kandri Rodi, M. Taleb, A. El Biache & Z. Rais, J. Appl. Electrochem. 51 (2021) 245-265.